

Ionization and harmonic generation in CO and H₂CO and their cations with ultrashort intense laser pulses with time-dependent density-functional theory

Emmanuel Fowe Penka, Etienne Couture-Bienvenue, and Andre D. Bandrauk*
Laboratoire de Chimie Théorique, Université de Sherbrooke, Quebec, Canada, J1K 2R1
 (Received 21 November 2013; published 12 February 2014)

Molecular high-order-harmonic generation and molecular-orbital ionization rates are calculated for the CO, H₂CO, CO⁺, and H₂CO⁺ molecules using numerical solutions of Kohn-Sham equations of time-dependent density-functional theory in the nonlinear nonperturbative regime of laser-molecule interactions. Different laser-molecule orientations ($\theta = 0, 90^\circ$, and 180°) and intensities (8.7×10^{13} , 3.5×10^{14} , and 1.4×10^{15} W/cm²) are used. Results show that at wavelength $\lambda = 800$ nm, the ionization rate maxima are influenced for each molecular orbital by the interplay between its ionization potential, its geometrical shape, and the laser polarization axis. Molecular high-order-harmonic generation is further studied by a time profile analysis and a time-dependent electron localization function. A comparison of the data between CO and H₂CO illustrates the importance of the protons on the electron distributions, ionization, and recollision dynamics in intense fields.

DOI: [10.1103/PhysRevA.89.023414](https://doi.org/10.1103/PhysRevA.89.023414)

PACS number(s): 32.80.Wr

I. INTRODUCTION

High-order-harmonic generation (HHG), the emission of high-energy photons resulting from the interaction of intense ultrashort laser pulses with atoms, has been extensively studied in recent years, offering potential application as a source of coherent ultrashort radiation in the extreme ultraviolet and soft-x-ray regions [1,2]. For molecules, molecular high-order-harmonic generation (MHOHG) [3] offers the possibility of synthesizing attosecond pulses ($1 \text{ as} = 10^{-18} \text{ s}$) with linear polarization [4], circular polarization [5], and controlling coherent electron wave packets [6,7]. An intuitive and simple theoretical picture based on the classical three-step electron recombination trajectory [8,9] in the laser field has helped to elucidate this process. According to this model, an electron tunnels out from the atom or molecule and may recombine with the parent [8,10] or neighboring [11] ion (emitting a high-energy photon), after undergoing laser-driven motion in the continuum. If the tunneling electron under the laser field does not return to the parent ion position, it is completely ionized and this is referred to as molecular ionization. The electron can also recombine with a neighboring ion at large distance, an example of laser-induced electron transfer [12].

Theoretical and experimental work on HHG has been mostly devoted to atoms. The study of MHOHG in molecules is at the early stages as it requires prealignment of molecules. In contrast to atoms, for molecules, the returning wave packet in the semiclassical picture of atomic HHG encounters a core comprising two or more nuclei, which are presumed to behave as pointlike source potentials leading to interference in the MHOHG spectrum. Additionally, it has been suggested that the electron recollision cross sections responsible for MHOHG relates to the projection of the valence orbitals with respect to the direction of the propagation of the recolliding electron, making possible a molecular-orbital tomography or holography [13,14]. While theoretical approaches based on the accurate three-dimensional (3D) time-dependent Schrödinger equation are limited to one-electron systems [13,15] and

2D models for two-electron systems in Born-Oppenheimer and non-Born-Oppenheimer simulations [16] because of a limitation of memory and computational time, the major difficulties in the theoretical study of molecular systems in a laser field reside in the multicenter nature of the molecule and the treatment of the multielectron-electron interactions in bound and continuum states. Here we focus on time-dependent density-functional theory (TDDFT) methods beyond linear response theory as a tool for studying the nonperturbative response of molecules to intense ultrashort laser pulses [17]. The time-independent density-functional theory (DFT) has become a ubiquitous method [18] of solving ground-state electronic problems in atoms and molecules. A time-dependent generalization of DFT was provided by Runge and Gross [19], showing that there is a one-to-one correspondence between the external (time-dependent) potential $v_{\text{ext}}(r,t)$ and the time-dependent one-electron density $n(r,t)$ for many-body systems evolving from a fixed initial state. The time-dependent electronic density for a closed-shell system is

$$n(r,t) = \sum_{\sigma=\uparrow,\downarrow} n_{\sigma}(r,t) = \sum_{\sigma=\uparrow,\downarrow} \sum_i^{N_{\sigma}} |\psi_{i\sigma}(r,t)|^2, \quad (1)$$

where $N_{\sigma} = N_{\downarrow}, N_{\uparrow}$ is the number of occupied orbitals for a given spin σ and $\psi_{i\sigma}(r,t)$ is the occupied orbital obtained through the time-dependent Kohn-Sham (KS) equations (in a.u.)

$$i \frac{\partial}{\partial t} \psi_{i\sigma}(r,t) = \left[-\frac{1}{2} \nabla^2 + v_{\text{eff}}(r,t) \right] \psi_{i\sigma}(r,t), \quad (2)$$

where

$$v_{\text{eff}}(r,t) = v_{\text{ext}}(r,t) + v_h(r,t) + v_{\text{xc},\sigma}(r,t). \quad (3)$$

The first term is the external potential, due to the interaction of the electron with an external laser field and the nuclei, the second term accounts for the classical Hartree electrostatic interaction between electrons, and the third is the exchange-correlation potential, which includes all nontrivial many-body effects and has an extremely complex (and essentially unknown) functional dependence on the density. Extension to

*andre.bandrauk@usherbrooke.ca

the nonperturbative regime through time-dependent methods has emerged by the existence of a rigorous theorem relating the exact time-dependent density to external time-dependent potentials [19]. To date, most highly nonperturbative nonlinear optical properties such as MHOHG have been observed in symmetric linear molecules for which only odd harmonics occur [20,21]. It had been shown earlier that for nonsymmetric molecules, the permanent dipole moment has a significant effect on enhanced ionization and MHOHG [15]. For the latter, even harmonics appear [15,22] and are subject to Coulomb focusing of electron wave packets [23]. Photoelectron angular distributions are then preferentially directed with respect to permanent dipoles [24,25]. Furthermore, with increasing intensity and longer pulses, inner-valence-shell multiple-orbital ionization occurs, thus complicating the interpretation of the tunneling ionization dynamics [26,27]. Such nonlinear nonperturbative effects appear now also in ionization and MHOHG of linear triatomics [28] and nonlinear molecules [29,30] and the general conclusion is that the geometrical shape of ionizing orbitals often determines the tunneling ionization rather than the ionization potentials

We present in this work numerical simulations of the nonlinear nonperturbative response of the CO and H₂CO molecules and their cations CO⁺ and H₂CO⁺ to short (few-cycle) intense laser pulses. The high-intensity ionization and MHOHG of CO have recently been examined experimentally in order to assess the importance of permanent dipole moments [31–34]. Multiorbital tunneling ionization of CO has been studied recently using elliptically polarized femtosecond laser pulses [32], thus confirming the earlier discovery of inner-shell ionization in ethylene [26] and N₂ [27] in intense fields. We compare the simple CO diatomic to formaldehyde, H₂CO, to investigate the effect of neighboring protons on the CO bond. Formaldehyde is one of the most abundant and ubiquitous molecules observed in the interstellar medium [35]. The formyl cation H₂CO⁺ is also a key ion in the medium and its photophysics has recently been investigated theoretically [36]. We focus therefore on the effect of protons on CO electrons in ionization and MHOHG. High-frequency imaging polyatomic molecules through photoelectron angular distributions has shown the importance of focusing of ionized electrons along bond direction [37]. We report such an effect with intense ultrashort pulses (800 nm) in H₂CO.

II. COMPUTATIONAL DETAILS

We compare by numerical simulations the nonlinear nonperturbative response of two polar molecules. The diatomic CO molecule, the tetra-atomic H₂CO molecule, and their cations are studied numerically using nonperturbative TDDFT. The method allows us to calculate Kohn-Sham orbitals whose energies are close to experimental ionization potentials (IPs) as these include density relaxations of the cation [38]. The method furthermore includes nonperturbative radiative coupling of inner orbitals during the laser pulses, thus allowing for a numerical estimate of the time-dependent evolution of all orbital populations during pulses. The TDDFT KS equation for each occupied molecular orbital (MO) in these molecules was discretized in space using finite-difference (FD) grid techniques as reported earlier for CO₂ and other

molecules [28,39]. We have used the van Leeuwen–Baerends (LB) [40] potential, which introduces a gradient correction to the local-density approximation (LDA) exchange correlation so as to reproduce correctly the Coulomb asymptotic behavior of the potential given as

$$v_x^{\sigma\text{LB}}(\mathbf{r}) = v_x^{\sigma\text{LDA}}(\mathbf{r}) - \beta n_\sigma^{1/3}(\mathbf{r}) \times \frac{x_\sigma^2}{1 + 3\beta x_\sigma \ln[x_\sigma + \sqrt{(x_\sigma^2 + 1)}]}, \quad (4)$$

$$x_\sigma = \frac{|\nabla n_\sigma(\mathbf{r})|}{n_\sigma(\mathbf{r})^{4/3}}, \quad \beta = 0.05. \quad (5)$$

The LB potential reproduces KS MO negative energies [28,41,42] nearly equal to the IPs obtained from photoelectron spectra, which are only accurately given normally by many-body Dyson orbitals [43]. Usually, the LB model potential ensures the correct Coulombic asymptotic behavior and gives good results for excitation and photoionization spectra [34]. When the laser is linearly polarized parallel to the molecular z axis, $v_{\text{ext}}(r, t)$ is given in the length gauge by

$$v_{\text{ext}}(r, t) = zE \cos^2(\pi t/T) \sin(\omega t). \quad (6)$$

Here T determines the laser pulse duration. The laser intensity is related to the field strength by $I = \frac{1}{2}\epsilon_0 c E^2$, ϵ_0 is the permittivity of free space and c is the speed of the light. The angle θ between the linear polarized laser and the main molecular z axis varies from 0 to 180°. The total pulse area condition $\int_{-\infty}^{+\infty} E(t) dt = 0$ is verified to ensure no spurious static effects for pulses satisfying Maxwell's equations [3,44]. The time-dependent equations (2) are solved using a Crank-Nicholson scheme with $\Delta t = 0.02$ a.u. (1 a.u. = 24×10^{18} s) as the time step and when the laser field is polarized along the z axis, a large 3D grid cell of dimension $|z_{\text{max}}| = 100$ a.u., $|y_{\text{max}}| = |x_{\text{max}}| = 40$ a.u. The uniform FD grid spacing $\Delta z = \Delta y = \Delta x = 0.36$ a.u. is used and the convergence of the calculations is checked against results making use of a smaller grid spacing. The spatial grid spacing guarantees the inclusion of moments up to the maximum: 1D $P_{\text{max}} = \pi/\Delta z = 9.5$ a.u. or the equivalent of the maximum energy $p^2/2 = 45$ a.u. All calculations are done using at least six optical cycles pulse duration on a multiprocessors parallel machine. Bonds length are set to their optimized neutral parameters value, i.e., the H₂CO and H₂CO⁺ geometry parameters are 0.192 nm for CO, 0.110 nm for CH, and 116° for HCH, whereas for the CO and CO⁺ molecules the parameter is 0.112 nm for CO. The CO bond is set to be parallel to the z axis as mentioned in our earlier work [28]. For each spin-orbital KS MO, the time-dependent ionization probability $P_{i,\sigma}(t)$ is calculated as [39]

$$P_{i,\sigma}(t) = 1 - N_{i,\sigma}(t),$$

where

$$N_{i,\sigma}(t) = \langle \psi_{i,\sigma}(r, t) | \psi_{i,\sigma}(r, t) \rangle \quad (7)$$

is the time-dependent population (survival probability) of the (i, σ) th spin population and a mask function is used to absorb ionized electrons at the grid boundary [28]. By using this technique, the KS wave function is multiplied at each time step at grid boundaries by a function $M(z)$, which is 1 in the inner

simulation region and gradually goes to 0 at the boundaries. The masking function in one dimension is defined as

$$M(z) = \begin{cases} \sin^{1/4} \left(\frac{z_{\max} - |z|}{2a} \pi \right) & \text{for } z_{\max} - |z| < a \\ 1 & \text{otherwise.} \end{cases} \quad (8)$$

Here $|z_{\max}| = 90$ a.u. is the extension of the box in the z direction, a is the width of the mask function, and we assume that the electrons in the $z_{\max} > |z|$ domain are completely ionized and cannot return to the nuclei. The position of the absorber is determined by the size of the maximum excursion $\alpha = E/\omega^2$ of an ionized electron in a static field of amplitude E and frequency ω . Thus, at intensity $I = 3.5 \times 10^{14}$ W/cm² (10^{-2} a.u., i.e., $E = 0.1$ a.u.) and for $\lambda = 800$ nm (i.e., $\omega = 0.0569$ a.u.), $\alpha = 31$ a.u. = 1.6 nm. The power spectrum for the MHOHG $S_z(\omega)$ in a given direction yields the predicted MHOHG spectra and can be computed from the time-dependent dipole $d_z(t)$, which for intense fields, due to the complete state numerical approach, yields the same results in other gauges [3]

$$S_z(\omega) = \left| \int d_z(t) e^{i\omega t} dt \right|^2. \quad (9)$$

The profile analysis has been used to get insight into the recollision process as proposed in the Corkum three-step models [8–10]. It is obtained from the following Fourier-Gabor transform:

$$d_G(\omega, t) = \int_{-\infty}^{+\infty} \exp(-i\omega t') \exp\left(-\frac{(t' - t)^2}{\sigma_0^2}\right) d_z(t') dt'. \quad (10)$$

Here $\sigma_0 = 0.1$ fs is the width of the Gaussian time window in the Gabor transform. In the frequency domain it corresponds to a Gaussian frequency filter with a spectral width equal to 10ω , where $\omega = 0.0569$ a.u. ($\lambda = 800$ nm) is the laser frequency. The resulting time profile indicates the time at which the selected set of harmonics was emitted during the laser pulse and therefore is considered as electron recollision times [8,9].

III. MOLECULAR-ORBITAL IONIZATION

In Fig. 1 we show the three highest occupied molecular orbitals HOMO, HOMO-1, and HOMO-2 of CO and CO⁺ (CO/CO⁺) and H₂CO and H₂CO⁺ (H₂CO/H₂CO⁺) as well as their computed KS energy and the corresponding available experimental IP [45–47]. The main observation is that the valence MOs of CO/CO⁺ are composed of one π and two σ MOs and each subsequent MO is separated by about 2ω at 800 nm ($\omega = 1.5$ eV). Those of H₂CO/H₂CO⁺ are composed of two π [$1b_1$ (x symmetry) and $2b_2$ (y symmetry)] orbitals with nodes along the C-O bonds and one σ [$4a_1$ (z -symmetry)] type of MO and the HOMO and HOMO-1 are separated by 2ω , whereas HOMO-1 and HOMO-2 are separated by approximately 1ω , suggesting a one-photon resonance in the latter at 800 nm. The HOMO is of σ type for CO and of π type for H₂CO. Our calculations show that the LB potential that contains self-interaction and the correct asymptotic Coulomb form yields ionization energies that especially for the HOMO are in agreement with the available experimental IP, thus suggesting that we have the proper wave function [48] as the

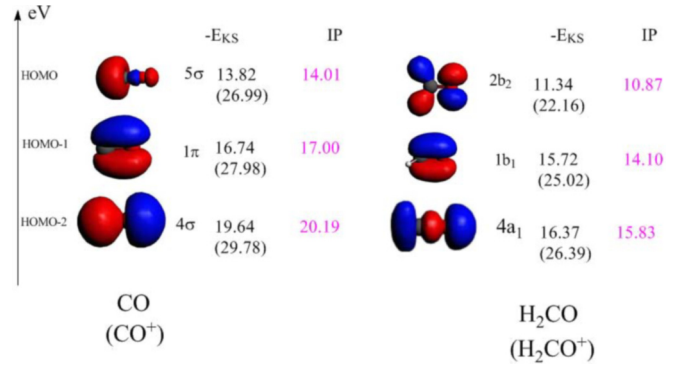


FIG. 1. (Color online) The DFT and LB images and energies of the KS molecular orbitals of CO and H₂CO and their cations (in parentheses). Only the three highest relevant occupied molecular orbitals, HOMO, HOMO-1, and HOMO-2, are shown with their energy E_{KS} and available IP for the CO molecule [45,46] and the H₂CO molecule [47].

starting point for our simulation as these include relaxation effects in the cation. Finally, the orbitals of CO/CO⁺ and H₂CO/H₂CO⁺ differ by the shape of their HOMOs (σ and π) and their IPs (13.82 and 11.20 eV).

In Fig. 2 we report the time evolution in intense fields of the above relevant KS orbitals as illustrated in Fig. 1 in zero field for CO, H₂CO, and their cations CO⁺ and H₂CO⁺. Three angular orientations $\theta = 0, 90^\circ$, and 180° with respect to the molecular z axis (CO bond) and to the laser polarization and two laser intensities $I = 3.5 \times 10^{14}$ and 1.4×10^{15} W/cm² were considered in Fig. 2 for CO and its cation CO⁺ and in Fig. 3 for H₂CO and its cation H₂CO⁺. The electric dipole moment of CO is calculated to be -0.108 D (C⁻O⁺), in agreement with the experimentally observed [49] value of -0.12 D (C⁻O⁺). One finds also that $\mu_{CO^+} = 1.11$ D, which confirms that the charge density is more diffuse behind the C atom in CO and the O atom in CO⁺ as seen in Fig. 1. In the latter, there is one less 5σ electron, which was localized around the C atom, thus resulting in more net charge on O in CO⁺. For H₂CO and H₂CO⁺, the permanent dipoles are $\mu_{H_2CO} = 2.73$ D (2.33 D in [50]) and $\mu_{H_2CO^+} = 3.64$ D. The dipole moments increase in the cations due to the removal of a HOMO electron, which is largely localized behind the C atom (see Fig. 1).

In Fig. 2(a) (CO/CO⁺) at $I = 3.5 \times 10^{14}$ W/cm², one finds that, independently of the laser polarization angle θ , the HOMO 5σ is the most affected by the field, as its ionization probability is higher in CO than in CO⁺ (due to their IP difference). By comparing MO ionization at $\theta = 0$ and 180° , one sees that the ionization rate of the MOs is almost unchanged, reflecting the weak influence of the molecular dipole as recently confirmed experimentally [32] with circular polarized pulses. Reference [32] nevertheless reports significant asymmetry in the ionization. This suggests that rotation of the ionized angular distributions by circularly polarized pulses may play an important role [51,52]. The HOMO-2 (4σ) instead of the HOMO-1 (1π) presents the second most important ionization rate in CO and CO⁺ in the presence of the field and the MO ionization starts after nearly 2.4 optical cycles. At $\theta = 90^\circ$, a perpendicular laser-molecule orientation, the HOMO-1 whose electron density has a node

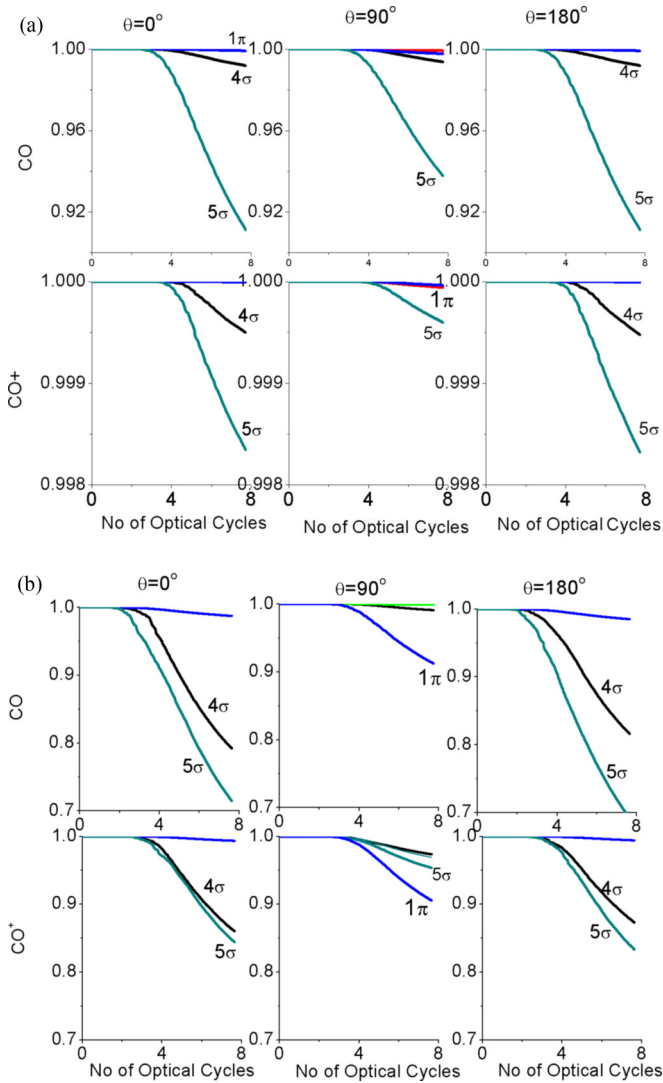


FIG. 2. (Color online) Orbital population $N_{i,\sigma}(t)$ [Eq. (8)] of CO and CO⁺ for different angles, $\theta = 0^\circ$, 90° , and 180° , between the main molecular z axis and the laser polarization, and for different laser intensities (a) $I = 3.5 \times 10^{14} \text{ W/cm}^2$ and (b) $I = 1.4 \times 10^{15} \text{ W/cm}^2$; the wavelength is 800 nm. The computed dipole moments are $\mu_{\text{CO}} = 0.108 \text{ D}$ and $\mu_{\text{CO}^+} = 1.11 \text{ D}$ for CO and CO⁺, respectively. Only the relevant KS orbitals are shown with their label.

along the molecular axis is not too much affected by the field in CO but is dominant in CO⁺. In general, one finds that due to its small IP, the HOMO presents the dominant response to the field at lower intensity and the ionization probability is generally higher for neutral CO than the cation CO⁺. Furthermore, since the HOMO and HOMO-1 are separated by 2ω energy, ionization from the inner orbitals (4σ and 1π) is not important for z polarization.

In Fig. 2(b) (CO/CO⁺) at higher intensity $I = 1.4 \times 10^{15} \text{ W/cm}^2$ ($4 \times 10^{-2} \text{ a.u.}$) our TDDFT and LB results show that both the HOMO 5σ and the HOMO-2 4σ present the dominant response to the field when $\theta = 0$ and 180° . One finds also that the ionization rate of the HOMO-2 4σ is comparable to the HOMO 5σ . For the perpendicular orientation $\theta = 90^\circ$, one finds that the ionization of the HOMO-1 1π is now dominant,

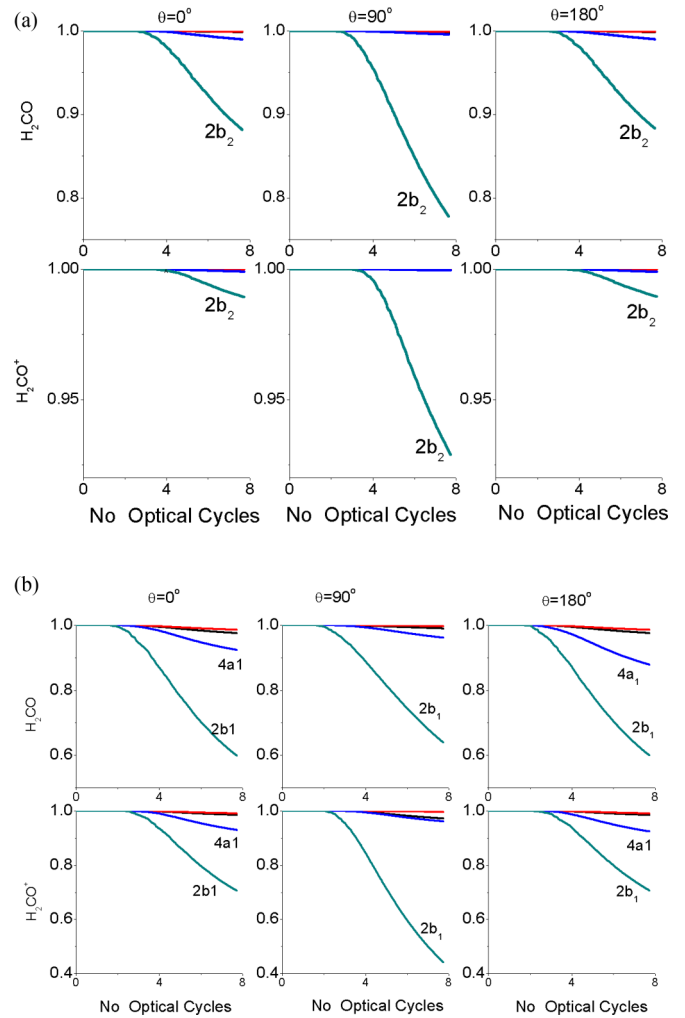


FIG. 3. (Color online) Orbital population $N_{i,\sigma}(t)$ [Eq. (8)] of H₂CO and H₂CO⁺ for different angles $\theta = 0^\circ$, 90° , and 180° , between the main molecular z axis and the laser polarization, and for different laser intensities (a) $I = 3.5 \times 10^{14} \text{ W/cm}^2$ and (b) $I = 1.4 \times 10^{15} \text{ W/cm}^2$, with $\lambda = 800 \text{ nm}$. Only the relevant KS orbitals are shown with their label. The computed dipole moment are $\mu_{\text{H}_2\text{CO}} = 2.73 \text{ D}$ and $\mu_{\text{H}_2\text{CO}^+} = 3.63 \text{ D}$.

unlike what we have in Fig. 2(a) at the lower intensity $I = 3.5 \times 10^{14} \text{ W/cm}^2$ where the HOMO 5σ ionization is the largest. This results from the effect of a large electron density along the laser polarization axis and thus reflects the important role of orbital shape when we increase the laser intensity as emphasized previously in CO₂, OCS, and CS₂ molecules [28]. Specifically for CO⁺, our results reveal that at higher intensities both the 4σ and 5σ ionization rates are nearly equal even though their energy gap is around 3 eV, corresponding to a two-photon transition. This results from the similar symmetry of the HOMO-2 4σ and HOMO 5σ with dominant electron population along the internuclear axis. Such nearly equal ionization rates should result in interfering MHOHG from each orbital, as suggested for CO₂ by Smirnova *et al.* [53].

For H₂CO/H₂CO⁺, all atoms are in the molecular YZ plane and the CO bond is along the z axis. We display the

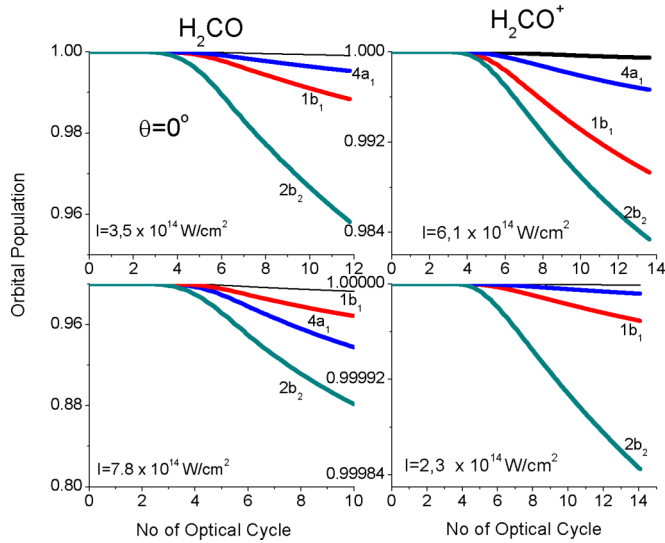


FIG. 4. (Color online) Orbital population $N_{i,\sigma}(t)$ [Eq. (8)] of H_2CO and H_2CO^+ for $\theta = 90^\circ$ (along the x axis) and different intensities $\omega = 800$ nm. Only the relevant KS orbitals are shown with their label. The computed dipole moments are $\mu_{\text{H}_2\text{CO}} = 2.73$ D and $\mu_{\text{H}_2\text{CO}^+} = 3.64$ D, respectively. The $2b_2$ (y -symmetry) HOMO dominates the ionization.

time-dependent MO populations for $I = 3.5 \times 10^{14}$ W/cm² [Fig. 3(a)] and $I = 1.4 \times 10^{15}$ W/cm² [Fig. 3(b)] laser intensities. The results show that the HOMO $2b_2$ (y symmetry) always presents the dominant response to the in-plane laser field followed by the HOMO-2 $4a_1$ (z symmetry) MO when $\theta = 0$ and 180° and by the HOMO-1 $1b_1$ when $\theta = 90^\circ$. For the neutral H_2CO molecule, the ionization of the inner MOs is negligible unlike in CO at parallel laser-molecule orientation, i.e., $\theta = 0$ and 180° . In H_2CO^+ , the HOMO $2b_2$ (y symmetry), even with a low electron density and two nodal planes (y and z) with respect to the laser field, presents the dominant response to the field, suggesting the important role that protons play in molecular ionization processes, and will be analyzed later using the time-dependent electron localization function (TDELf). Results also reveal that when the laser is polarized along the x axis, perpendicular to the molecular axis, the HOMO $2b_2$ presents the dominant response to the field and delocalization over the whole molecular yz plane (see Fig. 4).

As a concluding remark we note that the simulations indicate that the MO ionization process is influenced by the interplay between the IP, the orbital shape, and the laser polarization axis. In $\text{H}_2\text{CO}/\text{H}_2\text{CO}^+$, it is seen that IPs are lower due geometrically to more delocalization in the presence of protons and the corresponding MOs play the dominant role in the ionization. In fact, by comparing $\text{H}_2\text{CO}/\text{H}_2\text{CO}^+$ with the CO/CO⁺ molecule system, the IPs of $\text{H}_2\text{CO}/\text{H}_2\text{CO}^+$ are sufficiently weak such that tunneling ionization is favored even if MO densities are not aligned along the laser polarization axis. Also, in $\text{H}_2\text{CO}/\text{H}_2\text{CO}^+$, one notes also that, as illustrated in Fig. 2, the HOMO-1 $1b_1$ is indifferent to both the laser y - z polarization axis and intensity. This comes from the fact that the HOMO-1 $1b_1$ (of x symmetry) has its density minimal along the laser polarization axis (nodal plane in the molecular plane along the y and z axes). The KS HOMO ionization for

both H_2CO and CO and their cation increases with the laser field intensity and reaches a maximum depending on when the MO density either is optimal along the laser polarization axis or possesses the lowest IP. Overall, the $2b_2$ (y symmetry) HOMO with its large in y - z plane delocalization dominates the ionization process.

IV. MOLECULAR HIGHER-ORDER HARMONIC GENERATION AND TIME PROFILE ANALYSIS

In the previous section we illustrated the importance of the orbital IP, its geometrical shape, and the laser intensity on the MO ionization process. We noted that for intensity lower than 3.5×10^{14} W/cm², the HOMO has generally the dominant response to the field and the effect of the permanent dipole was found irrelevant when we compared the orbital ionization for the laser polarization $\theta = 0$ and 180° . We next examine the MHOHG spectral intensities of the neutral CO molecule [Fig. 5(a)] and the H_2CO [Fig. 5(b)] molecule for the two orientations $\theta = 0$ and 180° and at the lowest intensity $I = 8.7 \times 10^{13}$ W/cm². This lower intensity is used to minimize the contribution from inner orbitals and the maximum electron displacement $\alpha = E/\omega^2 = 15.3$ a.u. is well below the numerical grid size. This ensures that all recollisions are collected in our simulation and our study here is restricted only to the neutral molecules due to their small ionization potential. Results show that, in general, the overall shape of the power spectrum is similar for the two orientations (parallel and antiparallel). A cutoff that usually determines the highest harmonic order achievable and given by the classical law [8,10] $N\omega = P_{\text{ion}} + 3.17Up$ occurs as expected at the 20th harmonic for CO [Fig. 5(a)] and 15th for H_2CO [Fig. 5(b)]. In Fig. 5(a) (for CO), one notes that for the first eight harmonics, the spectrum intensity is independent of the laser polarization angle θ and odd harmonics exhibit higher intensity than the even ones. For harmonic order larger than the 7th, one sees that except for the 15th and 11th harmonics, even harmonic signal intensities in general are higher when $\theta = 0$ than when $\theta = 180^\circ$, thus reflecting a nonsymmetric charge distribution.

The MHOHG spectrum of H_2CO is presented in Fig. 5(b). As in Fig. 5(a), it also shows that the general shape is almost the same for the two laser orientations $\theta = 0$ and 180° . One finds that even harmonic signal intensities are generally higher than the odd ones and the overall signal intensity is higher when $\theta = 0$ than when $\theta = 180^\circ$; for example, the harmonic 13th intensity is nearly unobservable when the laser orientation is $\theta = 0$ where CO is in the z direction. For a better understanding of the effect of the molecular permanent dipole on the harmonic spectrum for the two orientations, we present the electron recombination dynamics or the time profile (10) of the ionized electron in Fig. 6(a) for CO and in Fig. 6(b) for H_2CO . Results show that, in general, harmonic signals are mainly generated by the recombinations of electrons around zeros of the electric field and their intensity increases with the external-electric-field amplitude. This suggests that highest-order harmonics are generated by recombination when the molecule is least perturbed by the electric field, whereas lower-order harmonics are generated when both the parent ion and the neutral molecule are strongly perturbed by the laser pulse. Furthermore, lower-order harmonics (lower

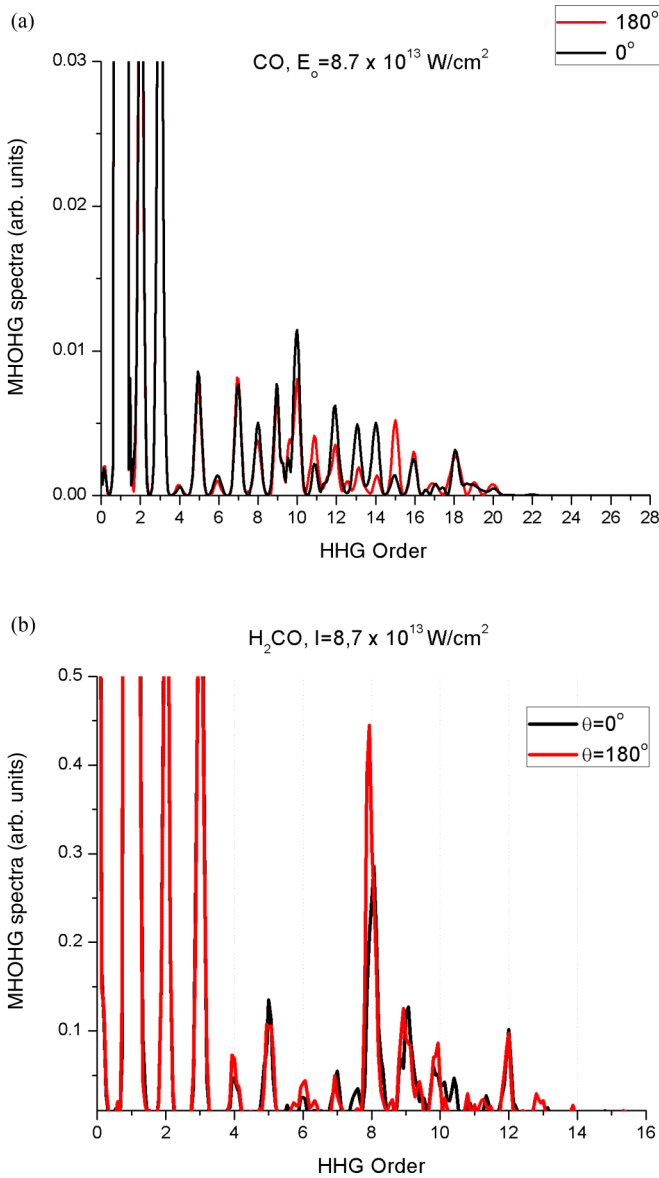


FIG. 5. (Color online) (a) The MHOHG (9) spectra of CO for fixed angles $\theta = 0^\circ$ and 180° between the molecular axis and the laser polarization direction. The peak intensity $I = 8.7 \times 10^{13}$ W/cm 2 and $\lambda = 800$ nm. (b) The MHOHG (9) spectra of H $_2$ CO for fixed angles $\theta = 0^\circ$ and 180° between the molecular axis and the laser polarization direction. The peak intensity $I = 8.7 \times 10^{13}$ W/cm 2 and $\lambda = 800$ nm.

returning kinetic energy) exhibit, in general, a broad signal corresponding to the well-known long and short recollision trajectories [9,10], while a single peak is observable only for higher-order harmonics referring to the electron returning to the molecular core with the maximum energy. In Fig. 6(a) for CO, two recollisions are observable during each optical cycle. Higher-order harmonics are found generated mainly by recollision at zero field around 5, 5.5, and 6 optical cycles. One notices that signals are in general more intense for $\theta = 0$ than for $\theta = 180^\circ$, which reflects the (C $^-$ O $^+$) charge distribution and thus a different recollision since when the

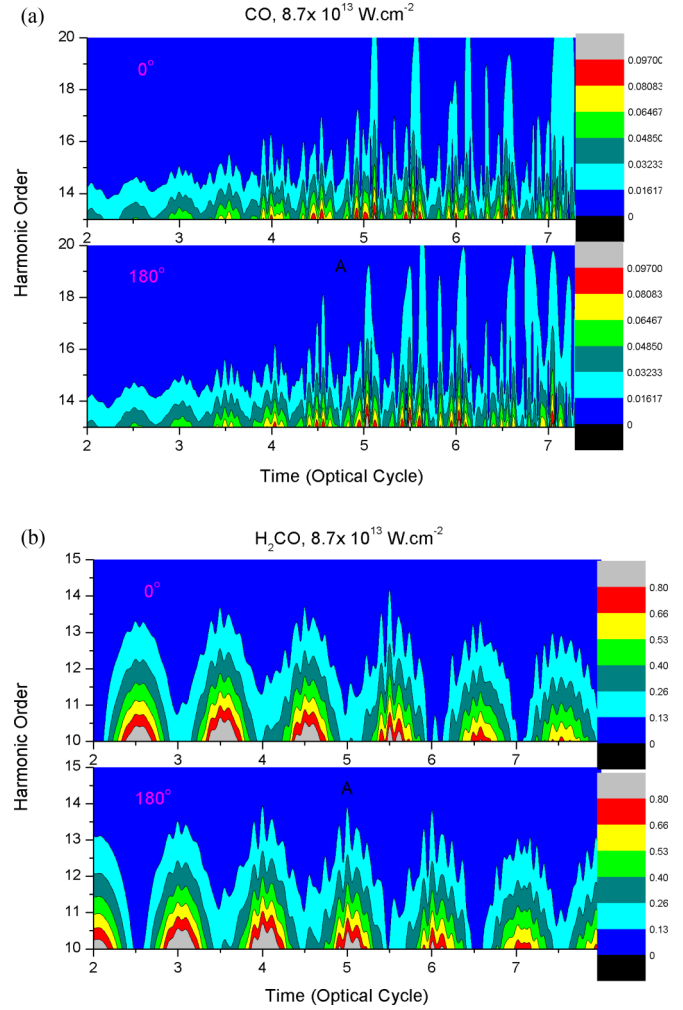


FIG. 6. (Color online) (a) Contour plot of the time profile (10) of the CO molecule obtained using the Gabor time windows defined in Eq. (6). (a) The top shows the result for $\theta = 0^\circ$. (b) The bottom shows the result for $\theta = 180^\circ$. The laser peak intensity $I = 8.7 \times 10^{13}$ W/cm 2 and $\lambda = 800$ nm. (b) Contour plot of the time profile (10) of the acceleration $dG(\omega, t)$ of the H $_2$ CO molecule obtained using the Gabor time windows defined in Eq. (6). (a) The top shows the result for $\theta = 0^\circ$. (b) The bottom shows the result for $\theta = 180^\circ$. The laser peak intensity $I = 8.7 \times 10^{13}$ W/cm 2 and $\lambda = 800$ nm.

electric field goes from positive to negative an electron goes from the negative direction to the positive.

In Fig. 6(b) we present the MHOHG time profile of H $_2$ CO. Unlike what we observe in Fig. 6(a) for CO, only one electron recollision is found during each optical cycle. The electron recollision also occurs at zero field, but at each $n + 0.5$ optical cycle (n is an integer) when $\theta = 0$ and each n optical cycle for $\theta = 180^\circ$. At the $n + 0.5$ cycle, the slope of the electric field is negative (i.e., decreasing field), whereas at n cycles, the slope is positive, corresponding to increasing electric field. The first case for $\theta = 0$ corresponds to ionization at a positive electric field and returning when the electric field is negative, whereas the last case for $\theta = 180^\circ$ corresponds to ionization at a negative electric field and returning at a positive electric field. The recollision therefore is unidirectional with the electron always ionizing away from the CH $_2$ moiety and returning along the CO

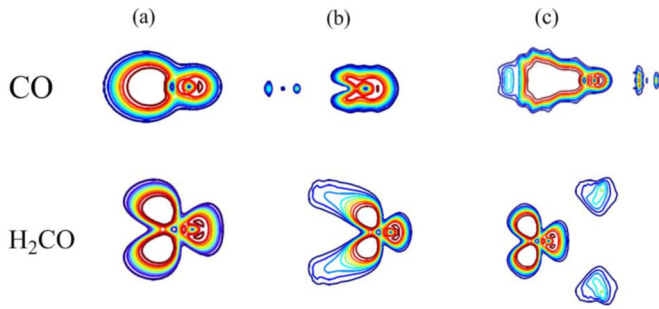


FIG. 7. (Color online) Contour plot of the TDELf CO and H_2CO molecules for $\theta = 0^\circ$ and (a) zero optical cycles, (b) after 4.25 optical cycles, and (c) after 4.75 optical cycles. The laser peak intensity $I = 8.7 \times 10^{13} \text{ W/cm}^2$ and $\lambda = 800 \text{ nm}$.

bond. For more analysis of this latter effect, we use the TDELf to determine the spatial evolution of an ionized electron.

The TDELf is a method for the mapping of the pair-electron probability in multielectron systems. It was first introduced by Becke and Edgecombe [54] as a descriptor of electronic localization, using arguments based on the conditional same-spin pair-probability function and extended for time-dependent processes by Burnus *et al.* [55]. Our recent work has shown that the electron localization function is a useful tool for identifying and visualizing the dynamics of lone-pair and bonding-pair electron ionizations in strong fields [56]. In the present work, TDELfs are used to compare in Fig. 7 the path followed by the ionized electron in CO and H_2CO when $\theta = 0$ and at different time steps. At zero field [Fig. 7(a)], in CO, TDELf images exhibit higher probability to localize an electron pair on the carbon atom than on the oxygen reflecting the negative dipole moment μ_{CO} (C^-O^+) and the extensive delocalization of the HOMO 5σ electron behind the C atom (Fig. 1). In H_2CO , a lone-pair electron is seen on the oxygen atom and a splitting of electron distribution with a higher TDELf value is found along each C-H bond due to the presence of the protons. The electron dynamic in the two molecules is analyzed and illustrated through two time steps: at 4.25 optical cycles for a maximal positive electric field, which leads to backward electron ionization away from the O atom [Fig. 7(b)], and finally at 4.75 optical cycles [Fig. 7(c)] for a negative maximal electric-field amplitude, which leads to forward electron ionization away from C. One finds that the ionization mechanism is quite different for the two molecules. In CO, the ionization follows the sp hybridization direction of the C-O bond while the forward-backward ionization in H_2CO results in two electron jets following the $2b_2$ (y -symmetry) ionization [HOMO (Fig. 1)] geometrical shape. As illustrated in Figs. 3 and 4, the H_2CO HOMO $2b_2$ dominates the

ionization at all intensities. However, the time profile analysis shows clearly that ionization occurs in one direction only, with the electron leaving the CH_2 region and then returning along the CO bond direction. This unique ionization-recollision path is dictated by the presence of the protons, i.e., the C-H bonds as seen in Fig. 7(b), which produce much larger electron delocalization as compared to CO. We point out that a similar phenomenon has been observed in direct high-frequency intense laser ionization of molecules with C-H bonds [37].

V. CONCLUSION

We have studied in this paper with TDDFT calculations the nonlinear nonperturbative effect of strong field on the linear CO and the planar H_2CO molecules and their cations. The main goal was to investigate under strong fields the molecular orientation effects and how the permanent dipole moment affects the electron ionization. This was done by analyzing the MO ionization rates, MHOHG spectra, the electron-nucleus recollision dynamics through time profiles, and electron ionization paths using the TDELf. As major results, we report that at equilibrium distance and at intensities $E > 3.5 \times 10^{14} \text{ W/cm}^2$, lower inner highest occupied molecular orbitals tend to contribute significantly to ionization due to the symmetry of these orbitals, even though they have higher IPs. In CO, ionization probabilities of different orbitals depend strongly on the laser-molecule orientation. The 1π HOMO-1 presents the dominant response to the field when the laser electric field is perpendicular to the molecular axis, whereas the HOMO 5σ , with maximum density along the molecular axis, is dominant for parallel orientation of the laser field and the orbital ionization is smaller at $\theta = 0$ than at $\theta = 180^\circ$. In H_2CO , the $2b_2$ HOMO, which is delocalized over all four atoms, presents the dominant response to the field independently of the laser intensity and the molecular orientation, an effect we attribute to its higher permanent dipole and its lower ionization potential. For weak laser intensity $E < 3.5 \times 10^{14} \text{ W/cm}^2$, our results reveal that the permanent dipole plays an important role in the electron-nucleus recollision scheme. The signal intensity is higher when $\theta = 0$ than when $\theta = 180^\circ$ and one finds during each optical cycle that two electron-nucleus recollisions occur in CO and only a single electron-nucleus recollision occurs in H_2CO . A comparison of TDELf images and time series analysis from CO to H_2CO shows that the protons influence strongly the ionization-recombination path. Thus, due to the large delocalization of the valence $2b_2$ HOMO over the protons, i.e., in the two C-H bonds, ionization occurs preferentially away from the CH_2 region followed by recollision along the C-O bond.

- [1] F. Krausz and M. Y. Ivanov, *Rev. Mod. Phys.* **81**, 163 (2009).
 [2] Z. Chang and P. Corkum, *J. Opt. Soc. Am. B* **27**, 9 (2010).
 [3] A. D. Bandrauk, S. Barmaki, S. Chelkowski, and G. L. Kamta, in *Progress in Ultrafast Intense Laser Science*, edited by K. Yamanouchi, G. Gerber, and A. D. Bandrauk (Springer, Tokyo, 2006), Vol. III.

- [4] K. Zhao, Q. Zhang, M. Chini, Y. Wu, X. Wang, and Z. Chang, *Opt. Lett.* **37**, 3891 (2012).
 [5] K. J. Yuan and A. D. Bandrauk, *Phys. Rev. Lett.* **110**, 023003 (2013).
 [6] A. D. Bandrauk, S. Chelkowski, H. Yu, and E. Constant, *Phys. Rev. A* **56**, R2537 (1997).

- [7] T. Bredtmann, S. Chelkowski, and A. D. Bandrauk, *Phys. Rev. A* **84**, 021401(R) (2011).
- [8] P. B. Corkum, *Phys. Rev. Lett.* **71**, 1994 (1993).
- [9] M. Lewenstein, P. Balcou, M. Y. Ivanov, A. L'Huillier, and P. B. Corkum, *Phys. Rev. A* **49**, 2117 (1994).
- [10] S. Chelkowski, G. L. Yudin, and A. D. Bandrauk, *J. Phys. B* **39**, S409 (2006).
- [11] F. Ding, W. Liang, C. T. Chapman, C. M. Isborn, and X. Li, *J. Chem. Phys.* **135**, 164101 (2011).
- [12] A. D. Bandrauk, S. Barmaki, and G. L. Kamta, *Phys. Rev. Lett.* **98**, 013001 (2007).
- [13] J. Itatani, J. Levesque, D. Zeidler, H. Niikura, H. Pepin, J. C. Kieffer, P. B. Corkum, and D. M. Villeneuve, *Nature (London)* **432**, 867 (2004).
- [14] X.-B. Bian and A. D. Bandrauk, *Phys. Rev. Lett.* **108**, 263003 (2012).
- [15] G. L. Kamta and A. D. Bandrauk, *Phys. Rev. Lett.* **94**, 203003 (2005).
- [16] A. D. Bandrauk, S. Chelkowski, S. Kawai, and H. Lu, *Phys. Rev. Lett.* **101**, 153901 (2008).
- [17] C. A. Ullrich and A. D. Bandrauk, in *Fundamentals of Time-Dependent Density Functional Theory*, edited by M. A. L. Marques, N. T. Maitra, F. M. S. Nogueira, E. K. U. Gross, and A. Rubio, Lecture Notes in Physics Vol. 837 (Springer, Berlin, 2012), pp. 357–374.
- [18] W. Kohn, *Rev. Mod. Phys.* **71**, 1253 (1999).
- [19] E. Runge and E. K. U. Gross, *Phys. Rev. Lett.* **52**, 997 (1984).
- [20] P. M. Kraus, A. Rupenyan, and H. J. Wörner, *Phys. Rev. Lett.* **109**, 233903 (2012).
- [21] A. Rupenyan, P. M. Kraus, J. Schneider, and H. J. Wörner, *Phys. Rev. A* **87**, 033409 (2013).
- [22] E. Frumker, C. T. Hebeisen, N. Kajumba, J. B. Bertrand, H. J. Wörner, M. Spanner, D. M. Villeneuve, A. Naumov, and P. B. Corkum, *Phys. Rev. Lett.* **109**, 113901 (2012).
- [23] T. Brabec, M. Y. Ivanov, and P. B. Corkum, *Phys. Rev. A* **54**, R2551 (1996).
- [24] M. Abu-samha and L. B. Madsen, *Phys. Rev. A* **82**, 043413 (2010).
- [25] X.-B. Bian and A. D. Bandrauk, *Phys. Rev. Lett.* **105**, 093903 (2010).
- [26] A. Talebpour, A. D. Bandrauk, J. Yang, and S. L. Chin, *Chem. Phys. Lett.* **313**, 789 (1999).
- [27] A. Becker, A. D. Bandrauk, and S. L. Chin, *Chem. Phys. Lett.* **343**, 345 (2001).
- [28] E. P. Fowe and A. D. Bandrauk, *Phys. Rev. A* **81**, 023411 (2010).
- [29] J. P. Farrell, S. Petretti, J. Förster, B. K. McFarland, L. S. Spector, Y. V. Vanne, P. Decleva, P. H. Bucksbaum, A. Saenz, and M. Gühr, *Phys. Rev. Lett.* **107**, 083001 (2011).
- [30] M. C. H. Wong, J.-P. Brichta, and V. R. Bhardwaj, *Phys. Rev. A* **81**, 061402(R) (2010).
- [31] Y. Liu, X. Liu, Y. Deng, C. Wu, H. Jiang, and Q. Gong, *Phys. Rev. Lett.* **106**, 073004 (2011).
- [32] J. Wu, L. P. H. Schmidt, M. Kunitski, M. Meckel, S. Voss, H. Sann, H. Kim, T. Jahnke, A. Czasch, and R. Dörner, *Phys. Rev. Lett.* **108**, 183001 (2012).
- [33] H. Du, L. Luo, X. Wang, and B. Hu, *Phys. Rev. A* **86**, 013846 (2012).
- [34] I. Znakovskaya, P. von den Hoff, S. Zherebtsov, A. Wirth, O. Herrwerth, M. J. J. Vrakking, R. de Vivie-Riedle, and M. F. Kling, *Phys. Rev. Lett.* **103**, 103002 (2009).
- [35] A. G. G. M. Tielens, *Rev. Mod. Phys.* **85**, 1021 (2013).
- [36] Å. Larson, M. Stenrup, and A. E. Orel, *Phys. Rev. A* **85**, 042702 (2012).
- [37] J. B. Williams *et al.*, *Phys. Rev. Lett.* **108**, 233002 (2012).
- [38] D. P. Chong, O. V. Gritsenko, and E. J. Baerends, *J. Chem. Phys.* **116**, 1760 (2002).
- [39] C. A. Ullrich and A. D. Bandrauk, in *Time-Dependent Density Functional Theory*, edited by M. A. L. Marques, C. Ullrich, F. Nogueira, A. Rubio, K. Burke, and E. K. U. Gross, Lecture Notes in Physics Vol. 706 (Springer, Berlin, 2006), pp. 357–374.
- [40] R. van Leeuwen and E. J. Baerends, *Phys. Rev. A* **49**, 2421 (1994).
- [41] M. Awasthi, Y. V. Vanne, A. Saenz, A. Castro, and P. Decleva, *Phys. Rev. A* **77**, 063403 (2008).
- [42] S.-K. Son and S. I. Chu, *Chem. Phys.* **366**, 91 (2009).
- [43] J. V. Ortiz, *Int. J. Quantum Chem.* **100**, 1131 (2004).
- [44] T. Brabec and F. Krausz, *Rev. Mod. Phys.* **72**, 545 (2000).
- [45] D. W. Turner, C. Baker, A. D. Baker, and C. R. Brundle, *High Resolution Molecular Photoelectron Spectroscopy* (Wiley, New York, 1970).
- [46] A. W. Potts and T. A. Williams, *J. Electron Spectrosc.* **3**, 3 (1974).
- [47] P. M. Guyon, W. A. Chupka, and J. Berkowitz, *J. Chem. Phys.* **64**, 1419 (1976).
- [48] M. Dauth, T. Körzdörfer, S. Kümmel, J. Ziroff, M. Wiessner, A. Schöll, F. Reinert, M. Arita, and K. Shimada, *Phys. Rev. Lett.* **107**, 193002 (2011).
- [49] C. A. Burrus, *J. Chem. Phys.* **28**, 427 (1958).
- [50] P. H. Vaccaro, A. Zabludoff, M. E. Carrera-Patiño, J. L. Kinsey, and R. W. Field, *J. Chem. Phys.* **90**, 4150 (1989).
- [51] K.-J. Yuan and A. D. Bandrauk, *Phys. Rev. A* **84**, 013426 (2011).
- [52] K.-J. Yuan, S. Chelkowski, and A. D. Bandrauk, *J. Chem. Phys.* **138**, 134316 (2013).
- [53] O. Smirnova, Y. Mairesse, S. Patchkovskii, N. Dudovich, D. Villeneuve, P. Corkum, and M. Y. Ivanov, *Nature (London)* **460**, 972 (2009).
- [54] A. D. Becke and K. E. Edgecombe, *J. Chem. Phys.* **92**, 5397 (1990).
- [55] T. Burnus, M. A. L. Marques, and E. K. U. Gross, *Phys. Rev. A* **71**, 010501(R) (2005).
- [56] E. F. Penka and A. Bandrauk, in *Coherence and Ultrashort Pulses Laser Emission*, edited by F. J. Duarte (InTech, Rijeka, 2011).